www.sphinxsai.com

ChemTech

International Journal of ChemTech Research
CODEN( USA): IJCRGG ISSN : 0974-4290
Vol.5, No.1, pp 220-231, Jan-Mar 2013

# Behaviour of Indian natural Baryte mineral

**B. Prameena[3], G. Anbalagan[1]*, V. Sangeetha[2], S. Gunasekaran[3] and G.R. Ramkumaar[3]**

**[1]PG and Research Department of Physics, presidency college, TN, Chennai-600005, India**
**[2]Department of Physics, DG VaishnavCollege, T N, Chennai – 600106, India**
**[3]PG and Research Department of Physics, pachaiyappa's college, TN, Chennai-600030, India**

***Corres. Author: prameenahepta@yahoo.in***

**Abstract:** The mineral Baryte has been investigated by X-ray diffraction, infrared, optical absorption and Thermo gravimetric analysis (TGA) studies. In X-ray diffraction, structure has been determined as orthorhombic. In FTIR the fundamental stretching and bending vibrations observed in the infrared region for Ba and $SO_4$.The optical absorption shows the presence of Fe in the mineral. EPR results in the presence of iron and presence of manganese in the mineral. The thermal decomposition behaviour was determined by means of thermogravimetric analysis (TGA) at different heating rates in nitrogen. The activation energies of the thermal degradation were calculated by four different methods: Coats-Redfern, Flynn-Wall, Kissinger, and Kim-Park. The Flynn-Wall and Kim-Park methods were the most suitable methods to calculate the activation energy.
**Keywords** : X-ray powder diffraction; FTIR, thermogravimetric analysis (TGA); Baryte.

## 1. Introduction

Baryte, or baryte, ($BaSO_4$) is a mineral consisting of barium sulfate(1). The *baryte group* consists of baryte, celestine, anglesite and anhydrite. Baryte itself is generally white or colourless, and is the main source of barium. Baryte and celestine form a solid solution $(Ba,Sr)SO_4$(2). Baryte is a sulfate of barium with chemical formula, $BaSO_4$ (BaO 65.7% and $SO_3$ 34.3%). Barytes contains little or no soluble salts and is insoluble in water and acid. Pure barytes is white opaque to transparent but impurities cause a wide variation in colour. It is chemically inert and has a high density. It crystallizes in normal class orthorhombic barytes type with rhombic dipyramidal symmetry. Its mainly used in oil industries, electronics, TV screen, glass, ceramics and medical applications. Its also used in car fillers and paint industry. Previously its been found that, the infrared absorption of barytes has been studied in the range 1µ to25µ using ten different specimen, belonging to 001 and 110 sections. The extension of the range of study beyond 16 has revealed the presence of fundamentals at 21.3µ (470 $cm^{-1}$) and 22.8µ (439 $cm^{-1}$) besides other absorption maxima. Also the laser induced, time-resolved luminescence technique is a suitable tool for the identification of rare-earths in baryte and the discrimination of their oxidation states. Along with the common $Eu^{2+}$ luminescence, the emission of $Eu^{3+}$was detected for the first time in baryte. There are at least two structural positions for $Eu^{3+}$ in baryte crystal lattice. FTIR spectroscopy, can be used for the identification of constituent materials of Cultural Heritage as far as they provide information about characteristic vibrational levels(3-9). Nevertheless, not all transitions between vibrational molecular levels are allowed. Some transitions can appear only in the infrared spectrum. The IR-or Raman-allowed or forbidden transitions are determined by the selection rules. Molecules with low symmetry, most of the vibrational modes appear in both the IR and Raman spectra, but, normally, with very different intensities, because the polarizability change for a vibration (which is a required selection rule for Raman scattering) differs from the dipolar moment change (a required selection rule for IR absorption) for the vibration (10,11). Thus, the vibrational information obtained by IR spectroscopy (12). Crystals commonly have tabular habit and some have prismatic, columnar, and sometimes globular, massive, rosette, fibrous, and crystal forms. The details of baryte mineral are as shown in the Table 1.

## 2. Experimental

The Baryte mineral were ground with an agate mortar and pestle. The powdered sample was sieved, and the particles with diameter smaller than 50 micrometer were submitted to XRD, FTIR, UV and TGA studies. XRD analysis were performed with a SEIFERT X-ray diffractometer with Cu Kα radiation (λ=1.54 A), Cu filter on secondary optics, 45 kV voltage and 20 mZ current. The powdered sample was mounted on a quartz support to minimize background. A Perikin-Elmer Spectrum one FT-IR spectrometer was used, and the samples were analyzed in KBr pellets. Spectra were traced in the range 4000 – 400 $cm^{-1}$, and the band intensities were expressed in transmittance(%).

The optical absorption spectrum of the sample was recorded using Varian Cary 5E UV-Visible-NIR spectrophotometer in the range 200 – 2500 nm by employing mull technique.

EPR spectrumwas recorded on a Bruker EMX Plus spectrometer with a Modulation Frequency of 100 kHz and 20 mW microwave power.

Thermal analysis were performed in a simultaneous TG-DTA (Netzsch STA 409) procedure. The temperature was increased from 30°-1000° C, at heating rates of 5°, 10°, and 20° C/min. Measurements were made in nitrogen atmosphere. Barytewas takenin the pellet state and the sample weight was about 13mg.

**Table 1. The morphology of the baryte mineral**

| Mineral | Formula | Space group | Cell constants | | | Volume |
|---|---|---|---|---|---|---|
| | | | a(Å) | b(Å) | c(Å) | $(Å)^3$ |
| Baryte | $BaSO_4$ | Pbnm Z = 4 | 8.886 ±0.026 | 5.479±0.025 | 7.203±0.049 | 350.74 |

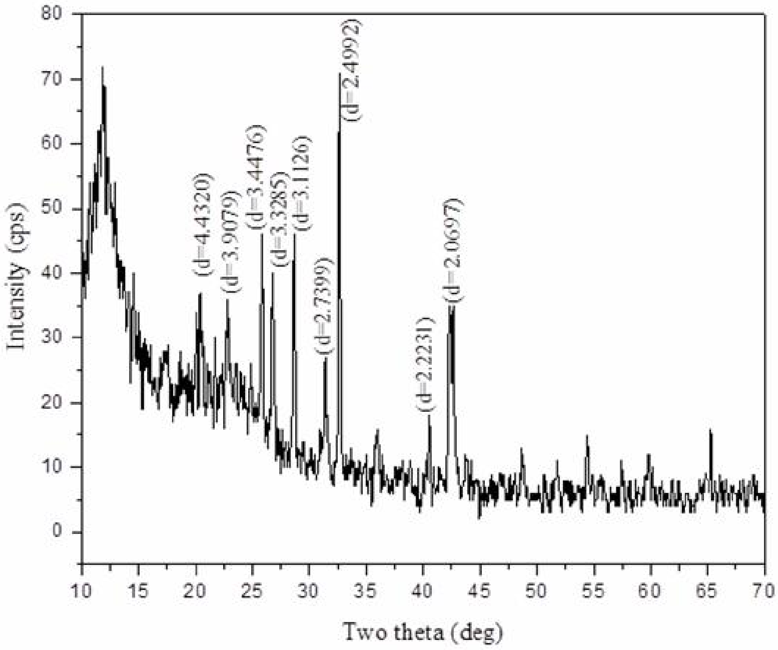


**Fig. 1X-ray Diffraction of baryte**

## 3. Results and discussion

### 3.1 X-ray diffraction analysis

The room temperature powder X-ray diffraction pattern of the baryte is given in Fig. 1 which shows quite sharp peaks with little background absorption. The presence of principal reflections at the d-spacings4.4320, 3.9079, 3.4476, 3.3285, 3.1126, 2.7399, 2.4992, 2.2231, 2.0697 Å indicates the presence of barytes and these readings are compared with JCPDS file No. 72-1390. It has an orthorhombic structure (pbnm), where S situated in tetrahedral coordination with O and Ba is surrounded by 12 oxygen's of 7 $SO_4$ tetrahedra(13). The $BaO_{12}$ polyhedral and the $SO_4$tetrahedral are edge-bound. The $BaO_{12}$polyhedral are irregular; six of the Ba-O distances are 2.77-281 Å, and the other 6 – 2.91 – 3.32 Å, which suggests a "sheet" structure parallel to {001}.

### 3.2 FTIR spectral analysis

The FTIR spectrum of baryte are shown in Fig. 2. The sulfate group has 4 fundamental vibrational modes: one non-degenerate mode ($\nu_1$), one doubly degenerate mode ($\nu_2$), two triply degenerate mode($\nu_3$and $\nu_4$). The IR spectrum of baryte exhibits several significance bands.Two strong bands corresponding to asymmetric stretching and bending($\nu_3$ and $\nu_4$) and two weak ones corresponding to symmetric stretching and bending($\nu_1$ and $\nu_2$). Only one reference reports the presence of water in the IR spectrum of baryte at 3430 and 1650cm$^{-1}$ (14). All the spectra of the studied bartyes sample are dominated by an intense $\nu_1$ band (symmetric stretching of $SO_4$tetrahedra) at 982 cm$^{-1}$ for bartye. ADLEER & KERR (1965) (15) found spectral shifts of the stretching modes ($\nu_3$ and $\nu_4$) to lower frequencies with increasing cation mass, such as the case of substitution Ba for Sr. The FTIR studies support the suggestion that the baryte contain traces of calcite $\nu_1$(1083 cm$^{-1}$), which coincides with $\nu_3$ of the $SO_4$ group and $\nu_4$(634cm$^{-1}$) bands. The free $SO_4$ molecule belongs to the $T_d$ symmetry. Corresponding to each of the vibration of the free $SO_4$ molecule, one expects to find the number of vibrations in the crystalline state. The number and their respective symmetry properties can be found out according to the procedure outlined by Couture and Mathieu (16). The effect of the crystalline state on the free $SO_4$ oscillation is two-fold. The symmetry of a single $SO_4$ molecule is changed from the tetrahedral group $T_d$ to the monoclinic local symmetry Cs, lifting the degeneracies of the doubly and triply degenerate oscillations in this manner the four fundamentals of the free $SO_4$ molecule give nine fundamentals. Table 2 is band component analysis of the IR of baryte. The infrared (IR) spectra of baryte from different occurrences are characterized by relatively weak but strongly pleochroic absorption bands at 3435 and 2923 cm$^{-1}$. These bands are assigned to anti-symmetric and symmetric OH stretching vibrations of two types of $H_2O$ molecules localized on vacant Ba sites.

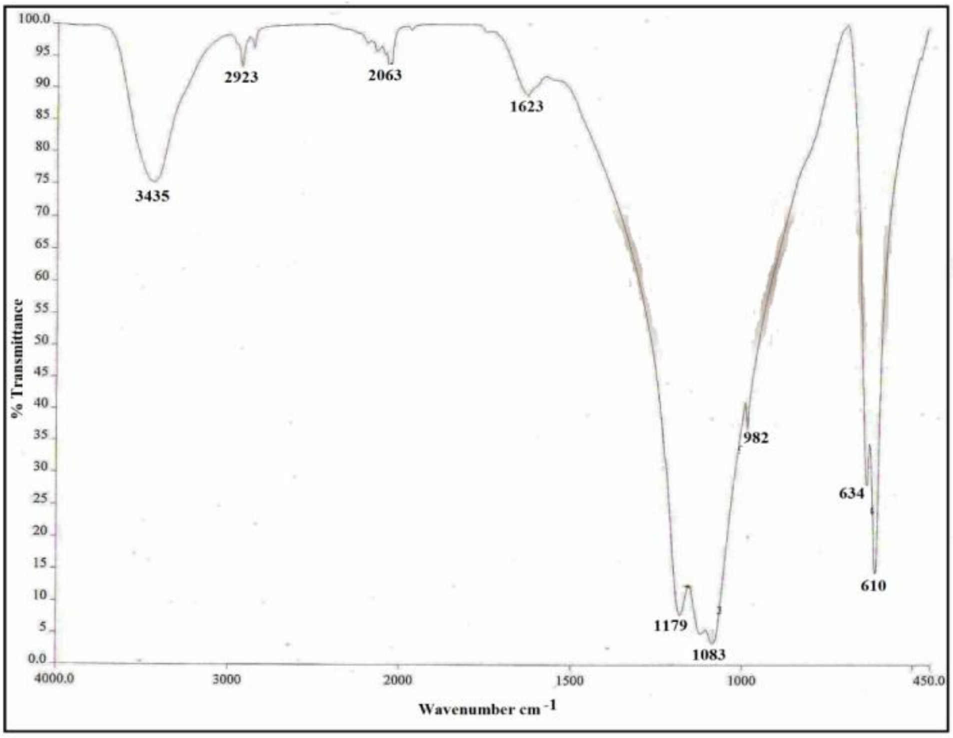


**Fig.2 FTIR spectrum of baryte**

**Table 2. FTIR Assignments of baryte**

| Sl.No. | IR | Assignment |
|---|---|---|
| 1 | 3435 | $\nu_3$OH |
| 2 | 2923 | $\nu_3$OH |
| 3 | 1623 | $\nu_3$ $SO_4$ |
| 4 | 1179 | $\nu_3$ $SO_4$ |
| 5 | 1083 | $\nu_1$ $SO_4$ |
| 6 | 982 | $\nu_1$ $SO_4$ |
| 7 | 634 | $\nu_4$ $SO_4$ |
| 8 | 610 | $\nu_4$ $SO_4$ |

one nondegenerate mode ($\nu_1$)
one doubly degenerate mode ($\nu_2$)
two triply degenerate mode($\nu_3$and $\nu_4$)

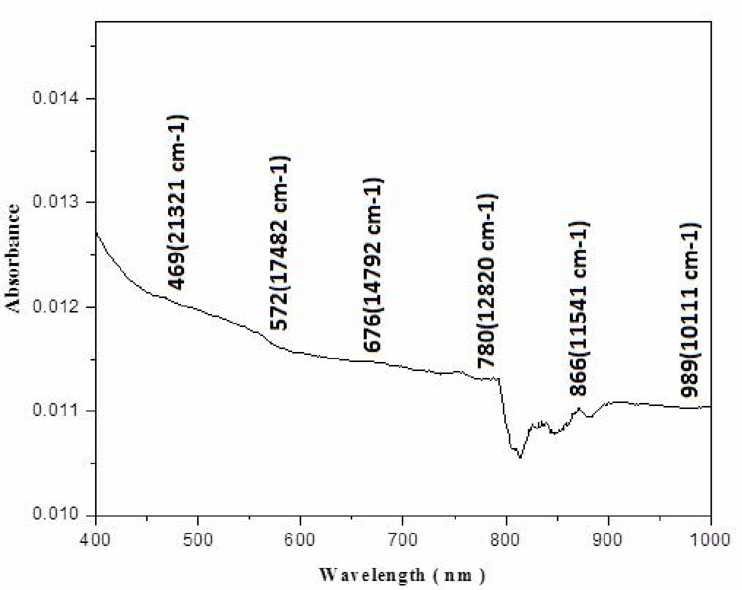


**Fig. 3 Optical absorption of baryte**

**3.3 Optical absorption spectrum**

The optical absorption spectrum (Fig. 3) exhibits features similar to those of $Fe^{2+}$ and $Fe^{3+}$ impurities in different iron bearing minerals (17-20). There are six bands observed in the spectrum and all are attributed to different transitions arising from isolated $Fe^{2+}$ and $Fe^{3+}$ as well as by pairs of iron ions. The bands observed at 14,792, 11,547 and 10,111 $cm^{-1}$.are characteristic of $Fe^{3+}$. The other four bands observed at 12,820, 17,482 and 21,321 $cm^{-1}$are assigned to $Fe^{2+}$.

***3.3.1 $Fe^{3+}$ ion***

The band observed at 11,541 $cm^{-1}$ is assigned to the transition ${}^6A_1 \rightarrow {}^4T_1({}^4G)$ and the band at 15,389 $cm^{-1}$ are assigned to the transition ${}^6A_1 \rightarrow {}^4T_2({}^4G)$ d-d transition as reported in the case of other samples(21,22). The transitions of other bands are assigned with the help of Tanabe-Sugano (1954)(23) diagram of $d^5$ configuration. From the ${}^6A_1 \rightarrow {}^4T_1({}^4G)$, ${}^6A_1 \rightarrow {}^4T_2({}^4G)$ transition energies and the Tanabe-Sugano equations (17), the ligand field theory parameters Dq, B and C are calculated.

***3.3.2 $Fe^{2+}$ ion***

Crystal field theory predicts that a d6 ion in an octahedral site will produce a single absorption due to the Lamporte-forbidden transition. The band observed at 10,111 $cm^{-1}$ corresponding to this transition ${}^5T_2 \rightarrow {}^4E(G)$ (24-26). Distortion of the octahedral site lifts degeneration of the d-orbitals and two or more absorption bands may occur. Reference(23) diagram of the d6 configuration is used to assign the transition to the other bands. The energy matrices of d6 configuration were solved for different values of Dq, B and C. The band positions, their assignments along with the calculated band energies are given in Table 3.

**Table 3. Optical absorption of bayte**

| Transition | Band position | | Calculated Wavenumber (cm-1) |
|---|---|---|---|
| | Observed | | |
| | Wavelength(nm) | Wavenumber ($cm^{-1}$) | |
| **For Fe(III) ion** | | | |
| **$^6A_1 \rightarrow {}^4T_1(^4G)$** | **866** | **11,111** | **11,319** |
| | **989** | **10,111** | **11,319** |
| **$^6A_1 \rightarrow {}^4T_2(^4G)$** | **676** | **14,792** | **15,389** |
| **For Fe(III) ion** | | | |
| **$^5T_2 \rightarrow {}^4T_1(^4H)$** | **780** | **12,820** | **11,640** |
| | **572** | **17,482** | **17,460** |
| **$^5T_2 \rightarrow {}^4E(G)$** | **469** | **21,321** | **21,771** |

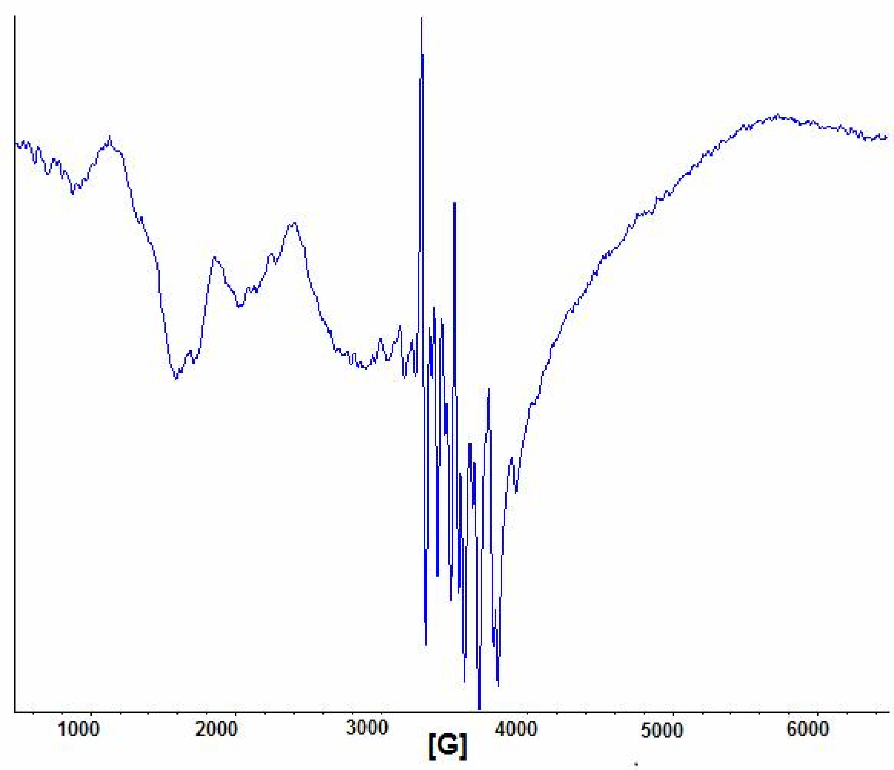


**Fig. 4 EPR Spectrum of barytes**

### 3.4 EPR spectrum

EPR spectrum of baryte at room temperature is given in Fig. 4. The observed wide range of g-values is attributed to $Fe^{3+}$ impurity in the lattice(27). If a trivalent ion replaces a divalent ion, the charge compensating vacancies will play an important role and can give rise to g-values ranging room 8-0.5, if the trivalent ion is $Fe^{3+}$ (26). Fig. 4 shows strong first derivate signals at g= 3.7., 6.38, 4.64 and smaller satellites near g=4.09 and 22.03. Except for the feature at g=22.03, these additional bands are correlated with the intensity of the pink color. A strong isotropic first derivative singal at g=3.3 along with weaker satellites at g=7.3, 6.2 (and possibly 5) should occur for$Fe^{3+}$ in a tetrahedral or axial environment(28).These theoretical values are close to the observed values at g =3.73, 4.68 and 6.38 in pink feldspars, indicating that this iron species are distinctly tetrahedrally coordinated $Fe^{3+}$. Hofmeister and Rossman (1984)(29) proposed that the axially-co-ordinated ion represents an intermediate state in deposition of hematite within the feldspar. The signal is probably not hematite itself because $Fe^{3+}$ interacts magnetically within the hematite unit cell and because of the previous observations of finely dispersed hematite in kaolin are associated only with broad resonances at g=2 (30). Divalent iron ions having six electrons in the outer shell with S=2 do not resolve in to resonance lines at normal conditions. If a trivalent ion replaces a divalent ion, the charge compensating vacancies will play an important role and can give rise to g-values ranging from 2.8 to 2.1. The additional bands are correlated with intensity of the pink color. The pink color results from small, dispersed hematite flakes, which suggests that these EPR features are associated with hematite or it precursors. It also shows the presence of manganese.

**3.5 Thermal analysis**

Thermogravimetric analysis (TGA) is commonly used to determine characteristics of thermal decomposition kinetics and thermal stability of baryte. Thermal decomposition kinetics of minerals can be investigated based on single heating rate and multiple heating rate methods (31,32). Methods used for calculating the kinetic parameters to characterize the thermal decomposition of the baryte which includes heating rate method, such as the Coats-Redfern methods, Flynn-Wall, Kim-Park and Kissinger methods (32). The heating rate method makes no assumption about the reaction order in the calculation of the activation energy. Although much research has been carried out into the physical properties and thermal behaviour of minerals, not much research and development has been carried out on the kinetic analysis of thermal decomposition of baryte. In this study, the kinetic analysis of thermal decomposition of barytewas investigated using TGA data obtained at different heating rates. The thermal stability and mechanism of thermal decomposition were considered. Multiple heating rate methods were used to calculate the activation energies of thermal decomposition and hence the advantages and disadvantages of each method are determined.

**TGA Kinetics Method of Thermal Degradation**: TGA kinetics analysis (33)is determined by measurement of fractional mass loss and degradation rate according to the temperature change. The fraction of conversion, α, is defined as:

$$\alpha = \frac{W_0 - W}{W_0 - W_f} \qquad (1)$$

where, W is the actual weight at any degradation time, $W_0$ is the initial weight, and $W_f$ is the final weight at the end of thermal degradation process. The rate of degradation, dα/dt, can be expressed as the product of the function of temperature and the function of conversion:

$$\frac{d\alpha}{dt} = \beta\frac{d\alpha}{dT} = k(T).f(\alpha) \qquad (2)$$

where β = dT/dt is the heating rate. If thermal degradation behaviour follows the Arrhenius equation, then k(T) is constant and the rate of degradation is expressed as:

$$k(T) = A\exp\left(-\frac{E_a}{RT}\right) \qquad (3)$$

where$E_a$ is the activation energy, A is a pre-exponential factor and R is the gas constant. It is assumed that the degradation reaction follows the $n^{th}$order reaction:

$$f(\alpha) = (1-\alpha)^n \qquad (4)$$

The combination of equations (2), (3) and (4) gives equations (5)

$$\frac{d\alpha}{dt} = \beta\frac{d\alpha}{dT} = (1-\alpha)^n A\, e^{-E/RT} \qquad (5)$$

Eq.(5) is integrated or differentiated to derive various equations for obtaining the kinetic parameters.

The multiple heating methods are used in this study to determine the thermal decomposition kinetics of baryteare as follows

**Coats-Redfern Method**

This method, as reviewed by Johnson and Gallagher (34)is an integral method that assumes various orders of reaction and compares the linearity in each case to select the correct order. The equations are given below.

By plotting the appropriate left-hand side of the below equations versus 1/T, the slope equals -E/2.303R.

$$\log\left[\frac{1-(1-\alpha)^{1-n}}{T^2(1-n)}\right] = \log\frac{AR}{\beta E}\left[1-\frac{2RT}{E}\right] - \frac{E}{2.303RT} \qquad for\ n \neq 1 \qquad (6)$$

$$\log\left[\frac{\log(1-\alpha)}{T^2}\right] = \log\frac{AR}{\beta E}\left[1-\frac{2RT}{E}\right] - \frac{E}{2.303RT} \qquad for\ n = 1 \qquad (7)$$

Thus a plot of either $\log_{10}[1 - (1 - \alpha)^{1-n} / (T^2(1 - n))]$ against 1/T (or) when n=1 $\log_{10}[-\log_{10}(1-\alpha)/T^2)$ against 1/T should result in a straight line of slope –E/2.3R for the correct value of n. Since it may be shown that for most values of E and for the temperature range over which the reactions generally occur the expression $\log_{10}AR/aE[1-2RT/E]$ is sensibly constant.

where E is activation energy of reaction and A is frequency factor.

The hydrations of natural baryte activated by using the TG data were evaluated in a four-step mechanism. Thedehydration activation energies of natural and acid activated montmorillonite samples were calculated (35). Theeffect of thermal treatment on some of the physico-chemical properties of the baryte was also investigated (36).In this study, our aim is to calculate the activation energy of dehydration of a barytesample.

**Flynn-Wall Method**

$$ln\beta = \ln\left(\frac{ZE_a}{R}\right) - lnF(\alpha) - \frac{E_a}{RT} \quad (8)$$

The Flynn-Wall method (37) is a simple method for determining activation energies directly from weight loss against temperature data obtained at several heating rates. The technique assumes that A, (1-α)n, and $E_a$ are independent of T, and that A and $E_a$ are independent of α. The value of the activation energy ($E_a$) can be calculated from the slope of the plot of lnβ versus 1/T for a fixed weight loss. This method cannot yield the other kinetic parameters except for the activation energy.

**Kim-Park Method**

$$ln\beta = lnZ + \left(\frac{E_a}{R}\right) + \ln\left[1 - n + \left(\frac{n}{0.944}\right)\right] - 5.3305 - 1.0516\left(\frac{E_a}{RT_{dm}}\right) \quad (9)$$

The Kim-Park method (38) assumes that $\alpha_m$ is independent of the heating rate, activation energy, and a pre-exponential factor. The activation energy is obtained by plotting lnβ against $1/T_{dm}$. Since the approximate value of the conversion factor used (0.9440), this technique can be more accurately usedto calculate the activation energy than the other methods, in which the value of the conversion factor is unity.

**Kissinger Method**

$$\ln\left(\frac{\beta}{T_{dm}^2}\right) = \ln\left[\frac{n(1-\alpha_m)^{n-1}ZR}{E_a}\right] - \frac{E_a}{RT_{dm}} \quad (10)$$

Here $T_{dm}$ is the absolute temperature at the maximum rate of thermal decomposition and $\alpha_m$ is the weight loss at the maximum decomposition rate. The Kissinger method (39) assumes that $\ln(1-\alpha m)^{n-1}$ is not dependent on the heating rate. It also assumes that the reaction order remains constant, and is very nearly equal to unity. The value of the activation energy can be calculated from the slope of the plot of $\ln(\beta/T_{dm})$ versus $1/T_{dm}$ at the maximum weight loss.

TGA experiments carried out in nitrogen atmosphere at the heating rates 5º C, 10º C and 20ºC is shown in Fig. 5.

Coats and Redfern method developed an integral method, which can be applied to thermogravimetric data, assuming the order of reactions. The correct order is presumed to lead to the best linear plot, from which the activation energy is determined. The first order equation was found to fit better. The straight line plots for baryte are given in Fig. 6, and the calculated activation energies are cited in Table 4.

The Flynn-Wall plots of lnβ versus 1/T for the baryte in nitrogen are shown in Fig. 7. The activation energies of thermal degradation for baryte under nitrogen and the calculated activation energies are cited in Table 5.Activation energies as calculated by the Kim-Park method are higher than that obtained by the Flynn-Wall method. The correlation coefficient of Kim-park method is lower than that of Flynn-Wall method.

Activation energies as calculated by Kim-Park method are closer to those obtained by the Kissinger method. Consequently, the Flynn-Wall method was more suitable. The kinetic parameters for the thermal decomposition of baryte in nitrogen as calculated from the Kim-Park and Kissinger methods are given in Tables 6 and 7 and are shown in Figs.8 & 9. The activation energies of baryte in nitrogen is61.127 & 64.051 $kJmol^{-1}$. Further, the activation energy and correlation coefficient values obtained from Kissinger method were higher than those from the Kim-Park method.

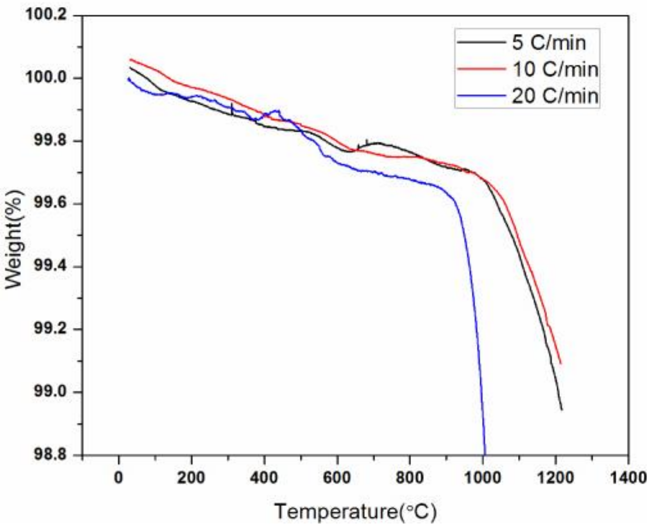


**Fig. 5 TG curves of baryte at various heating rates in nitrogen**

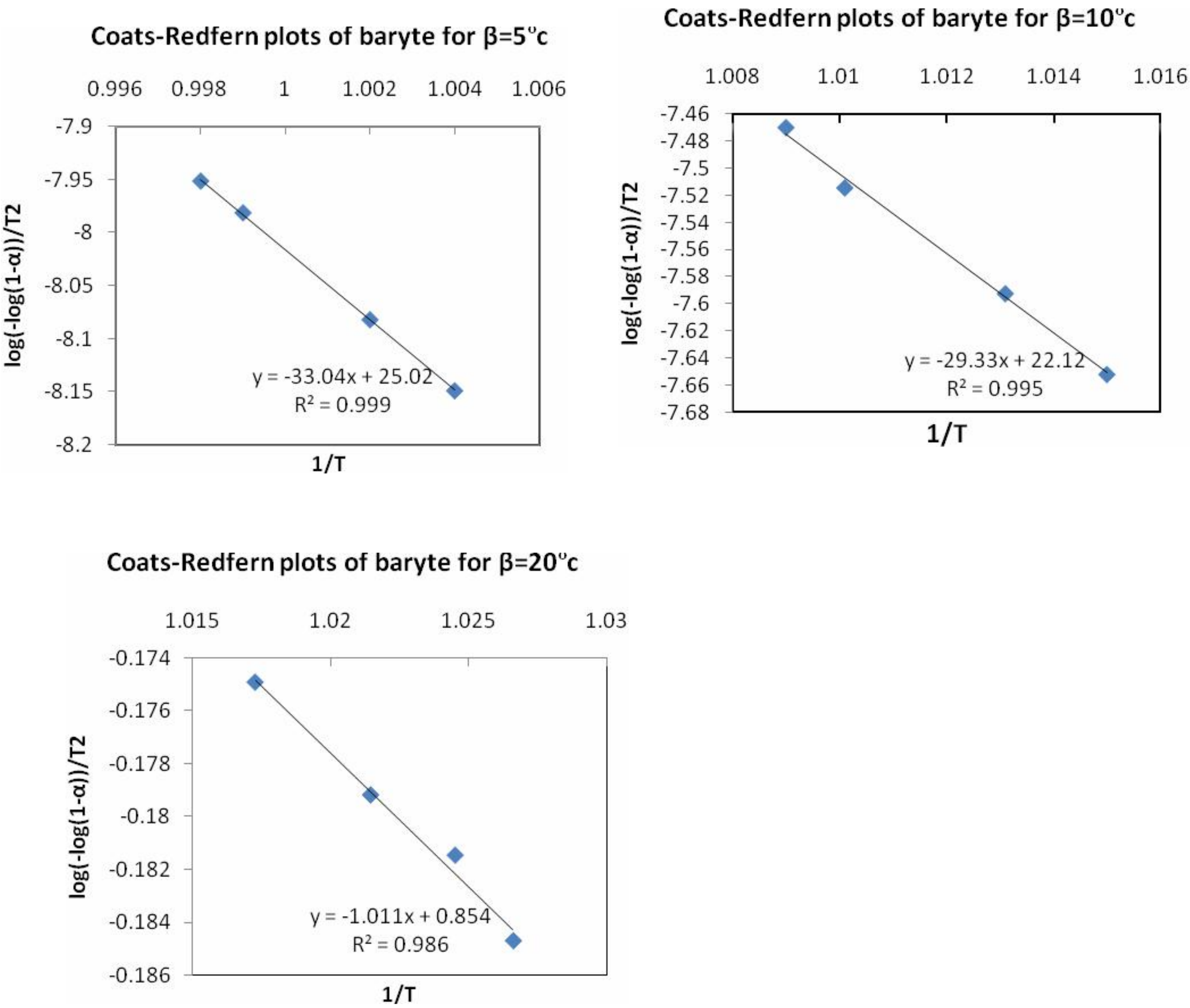


**Fig. 6 Coats-Redfern plots of baryte**

**Table 4. Activation Energies of Thermal Degradation for baryte under nitrogen obtained by the Coats-Redfern method**

| Temperature(°C) | Nitrogen | |
|---|---|---|
| | $R^2$ | $E_a$ (kJmol$^{-1}$) |
| 5° C | 0.9998 | 76.095 |
| 10° C | 0.9956 | 67.554 |
| 20° C | 0.9868 | 73.208 |

**Table 5. Activation Energies of Thermal Degradation for baryte under nitrogen obtained by the Flynn-Wall Method**

| Mineral | Nitrogen | |
|---|---|---|
| | $R^2$ | $E_a$(kJmol$^{-1}$) |
| Baryte | 0.99 | 76.445 |

**Table 6. Activation Energies of Thermal Degradation for baryte under nitrogen obtained by the Kim-Park Method**

| Mineral | Nitrogen | |
|---|---|---|
| | $R^2$ | $E_a$(kJmol$^{-1}$) |
| Baryte | 1 | 61.127 |

**Table 7. Activation Energies of Thermal Degradation for baryte under nitrogen obtained by the Kissinger Method**

| Mineral | Nitrogen | |
|---|---|---|
| | $R^2$ | $E_a$(kJmol$^{-1}$) |
| Baryte | 0.9998 | 64.051 |

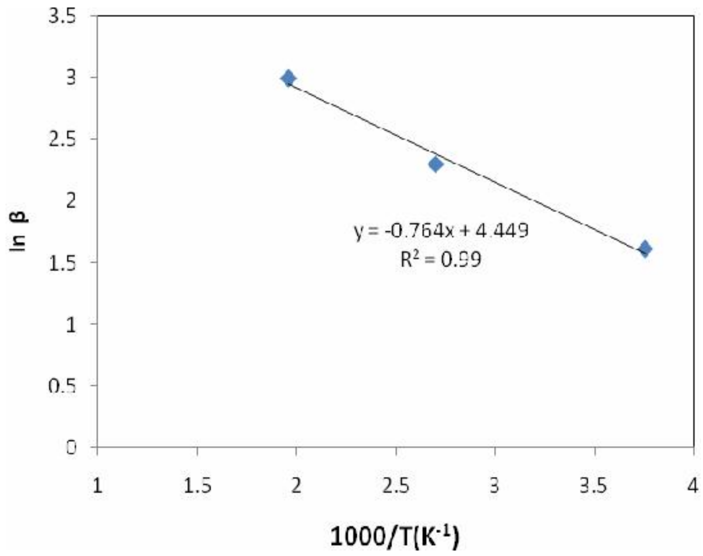


**Fig. 7 Flynn-wall method of baryte**

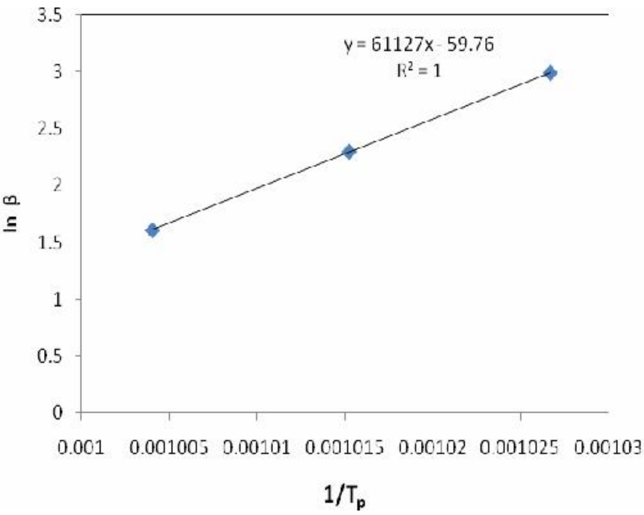


**Fig. 8Kim-Park method of baryte**

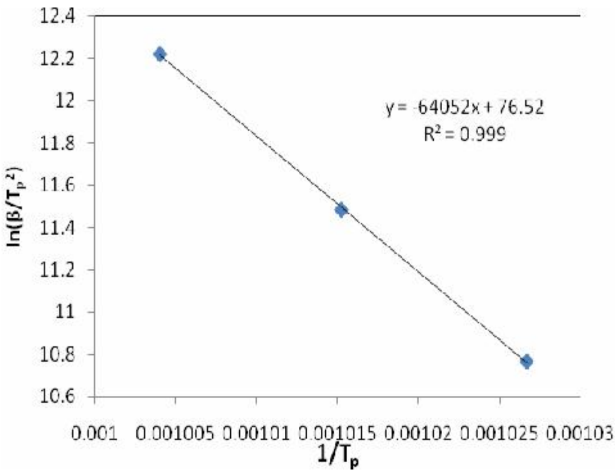


**Fig. 9Kissinger method of baryte**

## 4. Conclusion

In X-ray Diffraction the presence of principal reflections at the d-spacings 4.4320, 3.9079, 3.4476, 3.3285, 3.1126, 2.7399, 2.4992, 2.2231, 2.0697 Å indicates the presence of barytes. It has an orthorhombic structure (pbnm), where the S situated in tetrahedral coordination with O and the Ba is surrounded by 12 oxygens of 7 $SO_4$ tetrahedral. In FTIR, the sulfate group has 4 fundamental vibrational modes: one nondegenerate mode ($\nu_1$), one doubly degenerate mode ($\nu_2$), two triply degenerate mode($\nu_3$and $\nu_4$).The IR spectrum of baryte exhibits several significance bands. In optical absorption, Calcium and silicon bearing sulfates can display absorption bands when the atoms are linked through shared oxygens or hydroxide ions. Observed g-values around a range also confirmed in EPR spectrum. The thermal decomposition behaviour of barytewas investigated using TGA. It has good thermal stability of the mineral in nitrogen. The activation energies of thermal degradation were calculated by Coats-Redfern methods, Flynn-Wall, Kim-Park and Kissinger methods. It was found that the Kissinger, Kim-Park and Coats-Redfern methods were the most suitable methods to determine the activation energy.

## References


1. Dana, James Dwight; Ford, William Ebenezer,Dana's Manual of Mineralogy for the Student of Elementary Mineralogy, the Mining Engineer, the Geologist, the Prospector, the Collector, Etc. (13 ed.). John Wiley & Sons, Inc.. 1915, 299–300. http://www.archive.org/details/danasmanualmine00fordgoog.
2. Hanor, J., "Baryte-celestine geochemistry and environments of formation".Reviews in Mineralogy (Washington, DC: Mineralogical Society of America: Mineralogical Society of America),2000, 40, 193–275.
3. Castillejo, M., Martin, M., Silva, D., Anglos, D., Burgio, L., Clark, R.J.H,, J. Mol. Struct., 2000, 191–198.
4. Edwards, H.G.M., J. Mol. Struct.2003, 661–662.
5. Paternoster, G., Rinzivillo, R., Nunziate, F., Castelluci, E.M., Lofrumento, C., Zoppi, A., Felici, A.C., Fronterotta, G., Nicolai, C., Piacentini, M., J. Cult. Heritage,2005, 6, 21–28.
6. Civici, N., Denco, O., Clark, R.J.H., J. Culf. Heritage, 2005, 6, 157–164.
7. Andricopoulus, K.S., Daniilia, S., Roussel, B., Janssens, K., J. Raman, Spectroscopy, 2006, 37, 1026–1034.
8. Clark, R.J.H., J. Mol. Struct.,2007, 74–80.
9. Centeno, S.A., J. Shamir, J. Mol. Struct., 2008, 873, 149–159.
10. Levine, I.N., Molecular Spectroscopy, John Wiley and Sons Inc., New York, 1975.
11. Czernuszewick, R.S., Spiro, T.G., Chapter 7: IR Raman and Resonance Raman Spectroscopy, in: E.I. Solomon, A.B.P. Lever (Eds.), Inorganic Electronic Structure and Spectroscopy; Volume I: Methodology, John Wiley and Sons Inc., New York, 1999.
12. Clark, R.J.H., Mirabaud, S., J. Raman Spectrosc.2006, 37, 235–239.
13. James, R.W. & Wood, W.A., The crystal structure of barytes, Celestine and anglesite. Proceedings of the Royal society, 1925, 109A, 598-620.
14. Maya Dimova, Gerard Panczer and Michael Gaft, Spectroscopic study of baryte form the Kremikovtsi deposit (Bulgaria) with implication for its origin, 2006, 67, 101-108.
15. Adler, J.J. and Kerr. P.F., Variations in infrared spectra, molecular symmetry and site symmetry of sulfate minerals, American Minerelogist, 1965, 50, 132-147.
16. Couture and Mathieu, J. Phy.Rad., 1949, 10, 145.
17. Sherman, GD.M., WaiteT.D., Electronic spectra of Fe3+ oxides and oxide hydroxides in the near IR to near Uv. Am. Mineral, 1985, 70, 1262-1269.
18. Reece, J.J., Redfem, S.A.T., Welch, M.D., Henderson, C.M.B., C.A. McCammon, Temperature-dependent Fe2+ - Mn2+ order-disorder behavior in amphiboles. Phys. Chem. Miner, 2002, 29, 562-570.
19. Grygar, T., Dedeck, J., Kruiver, P.P., Dekkers, M.J., Bezdicka, P., Schnceweiss, O.,Iron oxide mineralogy inlate Miocene red beds from La Gloria, Spain; rock-magnetic, voltammetric and divisible spectroscopy analyses, Catena., 2003, 53, 115-132.
20. Taran, M.N., Monika, Koch-Muller, Langer, Klaus, Electronic absorption spectroscopy of natural (Fe2+, Fe3+)-bearing spinels of spinel S.S. – hercynite and gahnite solid solutions at different temperatures and high pressures, Phys. Chem. Miner, 2005, 32, 175-188.
21. Lakshman, S.V.J., Reddy, B., Optical absorption spectra of iron beryl, Spectrochim.Acta., 1970, 26A, 2230-2234.
22. Lehman, G., Harder, H., Optical spectra of di- and trivalent iron in corundum. Am. Mineral, 1970, 55, 98-105.
23. Tanabe, Y., Sugano, S., On the absorption spectra of complex ions, J. Phys. Soc. Jpn., 1954, 9, 753-779.
24. Gunasekaran, S., Anbalagan, G., Optical absorption and EPR studies on some carbonate minerals, Spectrochim. Acta., 2008, 69A, 383-390.
25. Narshima Reddy, S., Rao, P.S., Ravikumar, R.V.S.S.N., Reddy, B.J., Optical EPR and IR spectral studies of prehnite mineral, Ind, J. Phys, 2001, 75(A), 429-432.
26. Reddy, S.N., Ravikumar, R.V.S.S.N., Reddy, B.J., Reddy, Y.P., Rao, P.S., Spectroscopic investigations on Fe3+, Fe2+ and Mn2+ bearing antigorite mineral, N. Jb. Miner. Mh.2001, 6, 261-270.
27. Rao, P.S., Subramanian, S., Single crystal EPR studies of first-row transition ions inhexamidazole zinc (II) dichloride tetrahydrate IV, Iron (III); a case of strong tetrahedral distortion, Mol. Phys, 1985, 54, 415-427.
28. Golding, R.W., Singhasuwich, T., Tennat, T.W., An analysis of the conditions for an isotopic g-tensor in high-spin d5 systems, mol. Phys., 1977, 34, 1343-1350.
29. Hofmeister, A.M., Rossman, R., Determination of the $Fe^{3+}$ and $Fe^{2+}$concentratioins in feldspar by optical

abhsorption and EPR spectroscopy. Phys. Chem. Miner, H, 1984, 213-224.
30. Angel, B.R., Vincent, W.E., Electronspin resonance studies of iron oxides associated with the surface of kaolins, Clays Clay Miner, 1978, 26, 263-272.
31. Li, X.G and Huang, M.R, Polym. Int., 1998, 46, 289.
32. Li, X.G, J. Appl. Polym.Sci., 1999, 74, 2016.
33. Tonbul, Y., and Saydut, A., Thermal behavior and pyrolysis of Avgamasya Asphaltite., Oil Shale, 2007, 24(4), 547–560
34. Johnson, D.W..and Gallagher, P.K., J. Phys. Chem., 1972, 76, 1474-1477.
35. Guler, C., and Sarer, N., ThermochimicaActa, 1990, 159, 29-33.
36. Sarkaya, Y., Onal, M., Baran, B., and Alemdaro_glu, T., Clays and Clay Minerals, 2000, 48, 557-562.
37. Flynn, J.H., and Wall, L.A., Polym.Lett.,1996, 4, 323.
38. Kim, S., and Park, J.K., Thermochim.Acta, 1995, 264, 137.
39. Kissinger, H.E., Anal.Chem., 1957, 29, 1702.

*****